

Analysis of the Boundary Layer on a Highly Flexible Wing Based on Infrared Thermography Measurements

Mertens, Christoph; Grille Guerra, Adrián; van Oudheusden, Bas W.; Fehrs, Michael; Ritter, Markus R.

DOI

[10.1007/978-3-031-40482-5_1](https://doi.org/10.1007/978-3-031-40482-5_1)

Publication date

2024

Document Version

Final published version

Published in

Notes on Numerical Fluid Mechanics and Multidisciplinary Design

Citation (APA)

Mertens, C., Grille Guerra, A., van Oudheusden, B. W., Fehrs, M., & Ritter, M. R. (2024). Analysis of the Boundary Layer on a Highly Flexible Wing Based on Infrared Thermography Measurements. In *Notes on Numerical Fluid Mechanics and Multidisciplinary Design* (pp. 3-13). (Notes on Numerical Fluid Mechanics and Multidisciplinary Design; Vol. 154). Springer. https://doi.org/10.1007/978-3-031-40482-5_1

Important note

To cite this publication, please use the final published version (if applicable).
Please check the document version above.

Copyright

Other than for strictly personal use, it is not permitted to download, forward or distribute the text or part of it, without the consent of the author(s) and/or copyright holder(s), unless the work is under an open content license such as Creative Commons.

Takedown policy

Please contact us and provide details if you believe this document breaches copyrights.
We will remove access to the work immediately and investigate your claim.

Green Open Access added to TU Delft Institutional Repository

'You share, we take care!' - Taverne project

<https://www.openaccess.nl/en/you-share-we-take-care>

Otherwise as indicated in the copyright section: the publisher is the copyright holder of this work and the author uses the Dutch legislation to make this work public.



Analysis of the Boundary Layer on a Highly Flexible Wing Based on Infrared Thermography Measurements

Christoph Mertens¹(✉), Adrián Grille Guerra¹, Bas W. van Oudheusden¹,
Michael Fehrs², and Markus R. Ritter²

¹ Faculty of Aerospace Engineering, Delft University of Technology, Kluyverweg 1,
2629 HS Delft, The Netherlands

C.Mertens@tudelft.nl

² Institute of Aeroelasticity, German Aerospace Center (DLR), Bunsenstr. 10,
37073 Göttingen, Germany

Abstract. The effects of the wing skin distortion on the boundary layer of a highly flexible wing are analyzed in a wind tunnel experiment using infrared thermography measurements. Considerable differences in the boundary layer flow are observed when comparing the sections of the wing near the ribs, where the design shape of the wing is preserved, and in between the ribs. At the spanwise locations between the ribs, the sectional wing shape distorts and triggers boundary layer transition close to the leading edge. The differences between the design behavior of the wing and the experimental results of the boundary layer analysis demonstrate the need for considering the skin deformation and its effects on the boundary layer flow when designing highly flexible wings.

Keywords: Pazy wing · laminar separation bubble · differential infrared thermography · wind tunnel test

1 Introduction

The Pazy wing is a recently introduced experimental benchmark geometry for highly flexible wing studies [1]. The purpose of the benchmark model design is to sustain very large deformations in wind tunnel experiments, with wingtip deflections above 50% of the span, to provide experimental validation data for the activities of the Large Deflection Working Group within the framework of the third Aeroelastic Prediction Workshop¹. Since the publication of the first measurement data of the Pazy wing geometry, the data have already been used as a reference in several studies that focus on the development of novel non-linear aeroelastic prediction models [2,3]. The wing model, shown in Fig. 1, is constructed from a 3D-printed chassis that forms the leading and trailing edges as well as the ribs, which have a NACA 0018 cross-sectional shape. The stiffness

¹ <https://nescacademy.nasa.gov/workshops/AePW3/public/wg/largedeflection>

of the wing is mainly provided by an aluminum spar plate that is glued inside the chassis. A thin Oracalight iron-on film is used as the skin and is applied to the chassis by thermal shrinking. This construction process does not preserve the design airfoil shape between the ribs due to the flexibility of the foil and therefore locally alters the aerodynamic shape of the wing from the design shape. The first experimental studies of the Pazy wing at the Technion were focused on measurements of the structural dynamics [1], and did not include any dedicated aerodynamic characterization that would permit the analysis of this shape alteration effect.



Fig. 1. Pazy wing installed vertically in the wind tunnel test section at the Technion [1]

A further experimental study with an adapted version of the Pazy wing geometry, the Delft-Pazy wing, has been conducted at TU Delft. This study was focused on combined structural and aerodynamic measurements in the wind tunnel using a particle tracking velocimetry approach [4]. Furthermore, surface measurements with an infrared camera were conducted to analyze the boundary layer on the wing. However, while the interpretation of the infrared thermography measurement data is straightforward for steady attached flows, the analysis of flows with separation is more challenging [5]. Additionally, the high degree of flexibility of the wing exposes it to vibrations and thus unsteady flow conditions, further complicating the analysis [6].

In this paper, the boundary layer on the suction side of the Delft-Pazy wing is analyzed based on infrared thermography measurements. The purpose of this study is to demonstrate and assess an experimental approach to describe the effect of surface deformation on the aerodynamics of highly flexible wing structures. To support the analysis of the experimental data, a computational fluid dynamics (CFD) analysis of the Delft-Pazy wing is performed to provide insight into the expected flow patterns. Subsequently, the infrared measurements are analyzed using state-of-the-art data analysis methods to infer the boundary

layer state at different angles of attack in steady as well as oscillating inflow conditions, produced by a gust generator.

2 Boundary Layer on the Delft-Pazy Wing

A CFD analysis using the DLR TAU-code [7] is performed to assess the aerodynamic differences that are expected to occur between the design shape of the Pazy wing and the actual Delft-Pazy wing geometry that was used in the wind tunnel tests. The first step in this investigation is to generate an accurate model of the shape of the Delft-Pazy wing to be used in the simulations. This is achieved by performing a 3D-scan of the wing in the laboratory, in unloaded conditions, using a FARO Quantum Max scanner arm (maximum permissible error below 0.1 mm)². The result of the shape scan is visualized in Fig. 2. Two cross-sectional slices of the scanned geometry are shown, section I between two ribs and section II on a rib, as well as one slice along the span at $x/c = 0.25$. The differences between the outer shape of the Delft-Pazy wing to the design shape are clearly visible, the maximum thickness of the wing section between the ribs is reduced by more than 10% compared to the reference NACA 0018 airfoil.

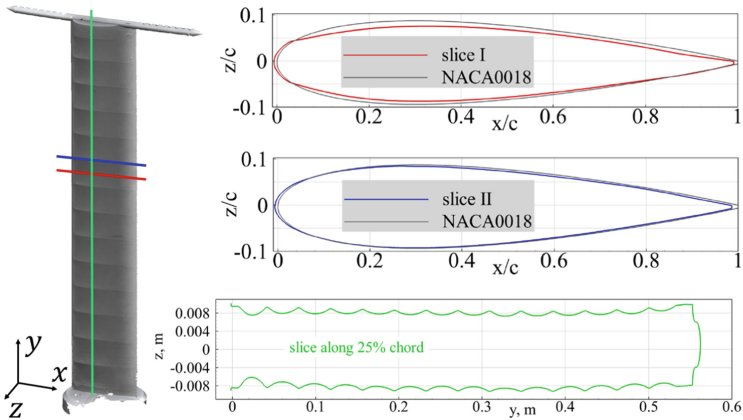


Fig. 2. Shape scan of the outer geometry of the Delft-Pazy wing

The shape scan data is further processed by generating a smooth geometry, correcting for imperfections of the shape scan due to gaps in the data, and afterward generating a grid for the CFD simulations. The CFD simulations are performed using the Reynolds-averaged formulation of the Navier-Stokes equations with the γ -model for boundary layer transition prediction [8]. Further details on the implementation of the CFD simulations can be found in [9].

² <https://www.faro.com/en/Products/Hardware/Quantum-FaroArms>

In Fig. 3, the results from the CFD simulations in terms of the skin friction coefficient distribution on the suction side at a chord-based Reynolds number of $Re = 340\,000$ and an angle of attack of $\alpha = 4^\circ$ are shown. On the left are the results for the design shape of the Pazy wing, and on the right, the results obtained for the scanned geometry of the Delft-Pazy wing are shown.

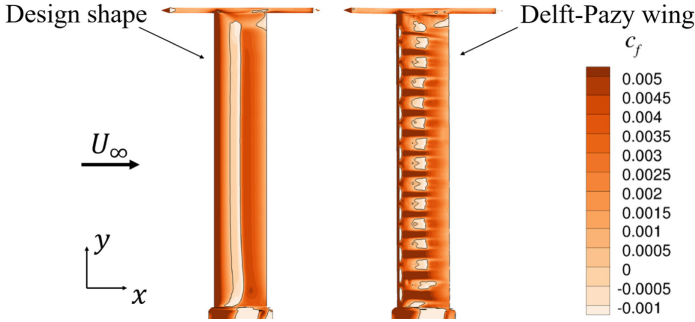


Fig. 3. Comparison of skin friction coefficient distributions at $\alpha = 4^\circ$ angle of attack

For the design shape, the flow is initially laminar, then separates at around $x/c = 0.3$ and reattaches at around $x/c = 0.45$, as indicated by the black lines. The increased skin friction level after the reattachment point indicates that transition to turbulence has occurred in the separated shear layer, thus forming a spanwise uniform laminar separation bubble (LSB). For the actual Delft-Pazy wing, a more complex boundary layer pattern is observed, with strong differences depending on the spanwise location. Near the locations of the ribs, the design airfoil is preserved well and the boundary layer flow closely resembles that of the design shape, forming a laminar separation bubble with a reattachment point around mid-chord. In between the ribs, the flow immediately separates downstream of the leading edge, at the kink in the sectional airfoil shape (originating from the chassis design of the Pazy wing, see Fig. 2). The flow then reattaches in a turbulent state at around $x/c = 0.1$ in the central part between the ribs. Closer to the ribs, a spanwise flow component from the rib to the sagged areas occurs, resulting in a pattern of consecutive separations in the chordwise direction. The occurrence of this complex behavior is verified experimentally in the following.

3 Experimental Setup

The infrared thermography measurements were performed at the Open Jet Facility wind tunnel at Delft University of Technology, which has a $2.85\text{ m} \times 2.85\text{ m}$ test section and a freestream turbulence intensity of around $Tu = 0.5\%$. The Delft-Pazy wing (chord $c = 0.1\text{ m}$, span $s = 0.55\text{ m}$) was mounted vertically in the wind tunnel test section and subjected to an inflow velocity of $U_\infty = 18.3\text{ m s}^{-1}$, corresponding to a Reynolds number of $Re = 122\,000$. The measurements were

performed with a FLIR SC7300 infrared camera, which was acquiring thermographic images of the suction side of the wing with a resolution of 320×256 pixels at a frame rate of 230 Hz, using an integration time of $250 \mu\text{s}$. The infrared camera measured the infrared radiation emitted from the surface of the wing, which is proportional to its surface temperature. To facilitate the analysis of the boundary layer state on the wing based on the thermographic measurements, the wing surface was heated above the temperature of the freestream with a halogen lamp.

The experimental setup and its components in the wind tunnel are shown in Fig. 4. The experimental conditions for the infrared measurements include steady inflow at angles of attack in the range $0^\circ < \alpha < 14^\circ$, as well as one test case with unsteady inflow conditions at $\alpha = 5^\circ$. With steady inflow, the wingtip reached a maximum tip displacement of 16% of the span. To generate the unsteady inflow, a gust generator was mounted upstream of the wing and operated continuously at a frequency of 5.7 Hz, corresponding to a reduced frequency of $k = f\pi c/U_\infty = 0.1$, and the amplitude of the sinusoidal inflow variation due to the gust was $\alpha_g = \pm 2.5^\circ$. The wing responded to this gust inflow with a sinusoidal oscillation with a small dynamic tip deflection amplitude of 1.5% of the span width, which was in anti-phase with the gust excitation phase angle ϕ [4].

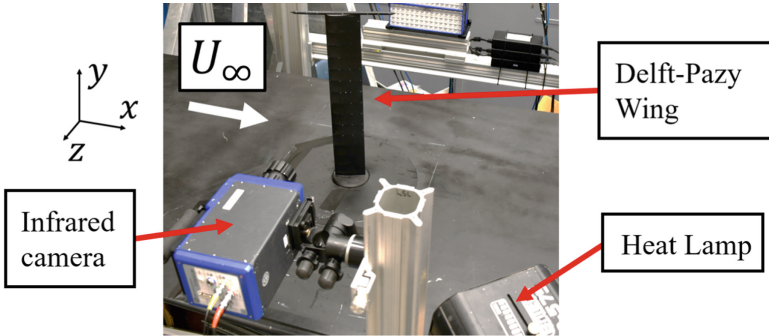


Fig. 4. Wind tunnel setup for the infrared thermography measurements

4 Infrared Thermography Data Analysis

The acquired infrared images are processed for the purpose of detecting of the boundary layer state. The physical values of the surface temperature are not required for this, hence no temperature calibration is performed and the data is analyzed in terms of the infrared radiation in camera counts. The infrared images are mapped onto the wing's reference system to account for the (dynamic) deflection of the wing by detecting the intersections of the ribs with the edges of the wing. For the steady inflow case, the field of view of the infrared camera

captures the full span of the wing. For each α , 100 images are taken for time-averaging. In the gust response situation, the spatial resolution is increased by capturing only a central region of the wing, covering 20% of the span.

The main features of a laminar separation bubble are the laminar separation, transition within the separated shear layer, and turbulent reattachment. In steady inflow, these features can be extracted from thermographic measurements by analyzing the chordwise temperature gradient [5]. Two examples of this approach are shown in Fig. 5, using data measured in the wind tunnel at $\alpha = 4^\circ$ for the two sections shown in Fig. 2.

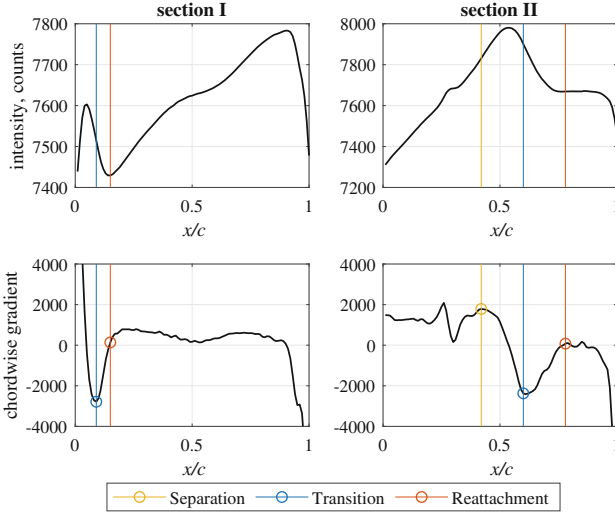


Fig. 5. Examples for the boundary layer state detection, for steady inflow at $\alpha = 4^\circ$

As the boundary layer thickness increases along the chord, the velocity gradient at the wall decreases. The skin friction is proportional to the velocity gradient and linked to the convective heat transfer through the Reynolds analogy. Therefore, the surface temperature is generally increasing with x for a wing that is heated above the temperature of the freestream. However, a turbulent boundary layer produces significantly larger skin friction values compared to a laminar boundary layer at the same Re_x . When transition occurs over a laminar separation bubble, the surface temperature is maximal inside the bubble, where the flow speed is lowest. The laminar-turbulent transition location is therefore considered to be the position of the minimum of the chordwise temperature gradient. The separation location can be determined as the position of the local maximum of the temperature gradient upstream of the transition location. When the flow reattaches, the chordwise temperature trend reverses from decreasing to increasing again. The reattachment location is therefore the position where the chordwise gradient becomes positive again. As observed in Fig. 5, the determination of the separation location with this approach fails when transition occurs

very close to the leading edge (section I), as there is no local maximum of the gradient. The detection of the reattachment is problematic when the laminar separation bubble is located further downstream (section II) because the non-uniformity of the external heating causes a reduction in the temperature increase near the trailing edge. Due to the challenges with determining the separation and reattachment locations, the quantitative results of this study are limited to the transition location x_{tr} , which is determined both on and between the ribs.

The aforementioned procedure can generally not be used in the case of unsteady inflow conditions. Here, the instantaneous surface temperature distribution may not directly correspond to the boundary layer state, as it will also be influenced by the thermal response of the surface material. To overcome this, differential infrared thermography (DIT, [6]) is applied for the identification of the unsteady transition location occurring on and next to the ribs of the wing. This technique consists of the subtraction of two thermograms obtained closely in time and the identification of unsteady features from the differential image. The approach is illustrated in Fig. 6. The small time separation between consecutive frames makes the two intensity distributions almost identical, but the application of DIT reveals a negative DIT peak linked to the transition process in the separated shear layer of an unsteady laminar separation bubble [10].

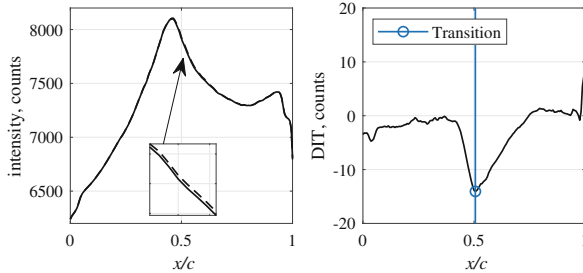


Fig. 6. Example of the identification of unsteady transition location using DIT

5 Results

The mapped and time-averaged thermographic images measured at eight angles of attack α in steady inflow conditions are shown in Fig. 7. For $\alpha = 0^\circ$, a region of increased surface temperature is present between $0.55 < x/c < 0.75$, which is relatively uniform along the span (the decrease in overall temperature for $y/s > 0.75$ can be attributed to the non-uniform external heating). The reduced convective heat transfer in this region can be explained by the presence of a laminar separation bubble. At $\alpha = 0^\circ$, the spanwise variation of the sectional shape of the wing has little influence on the boundary layer flow. However, as α increases, these variations cause differences in the spanwise flow pattern. The

main effect is a reduced surface temperature downstream of the kink near the leading edge in the airfoil shape between the rib locations. The kink causes the boundary layer to transition to turbulence, increasing the skin friction and thus the convective heat transfer when compared to a laminar boundary layer state. This effect sets in locally at individual spanwise locations at $\alpha = 2^\circ$, it is established along all spanwise sections at $\alpha = 4^\circ$, and further increases with increasing α . For very high values of α , the flow over the wing appears as fully turbulent at $\alpha = 12^\circ$, before at $\alpha = 14^\circ$ the wing stalls, causing an increased surface temperature at some sections of the span, in comparison to the turbulent attached flow. The high infrared count regions in the bottom part of the wing for the larger angles are measurement artifacts (reflections of the heat lamp).

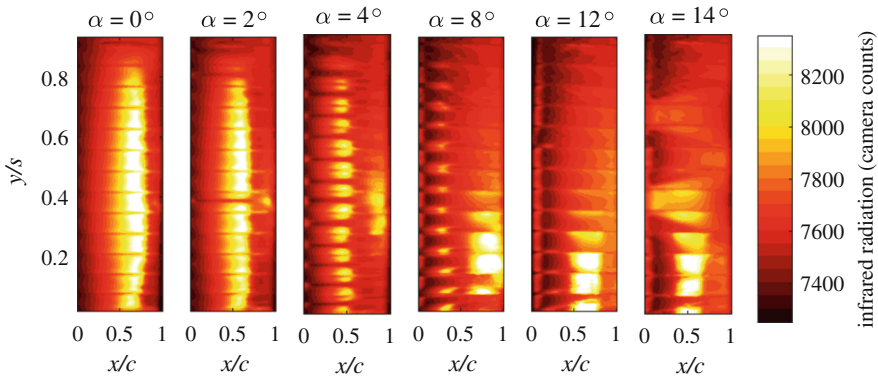


Fig. 7. Infrared images of the Delft-Pazy wing for $0^\circ < \alpha < 14^\circ$

The quantitative values of the extracted boundary layer transition location along the span are shown in Fig. 8. The locations of the ribs of the Delft-Pazy wing are indicated as well, showing that the boundary layer transition is triggered near the leading edge between the ribs for $\alpha \geq 4^\circ$. With increasing α and thus increasing adverse pressure gradients on the suction side of the wing, the transition location on the ribs moves gradually upstream and the region of turbulent flow covers a larger fraction of the span.

For analyzing the unsteady test case, the mapped infrared images are ordered in terms of the phase angle of the gust ϕ . Consecutive images are subtracted to create DIT images, and the unsteady transition location is identified from the mean DIT curve for 50 phase bins. This procedure is applied to every pixel row along the span that is close to the ribs of the wing. Between the ribs, transition remains approximately unaltered and close to the leading edge, as explained for the static measurements. The DIT peaks measured along the cycle next to a rib are shown in Fig. 9. Their sign changes depending on whether the transition location is moving upstream or downstream. This causes the appearance of two regions where no clear peak could be detected. To provide an estimation of the

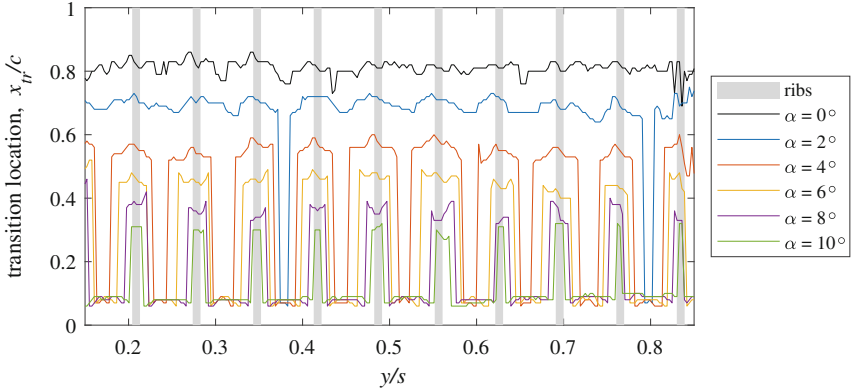


Fig. 8. Boundary layer transition location along the span for $0^\circ < \alpha < 10^\circ$

full cycle, a sinusoidal fit is constructed using the experimental data. From there, it can be observed that there is approximately a 10% lag between the motion and the unsteady transition process. Extending the approach along the span gives the unsteady transition fronts shown in Fig. 10, at five different phase angles along the cycle. The results indicate that the unsteady conditions have no effect in the region between ribs, while they induce variations in the transition location of more than 20% of the chord on and next to the ribs of the wing.

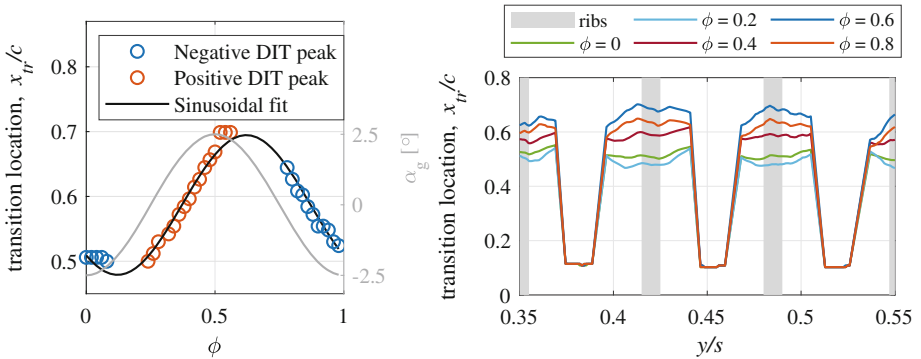


Fig. 9. Sinusoidal fit applied to the transition location measurements

Fig. 10. Unsteady transition location along the span for the sinusoidal gust response

6 Conclusion

The boundary layer that develops on the suction side of the highly flexible Pazy wing geometry was analyzed in this study based on infrared thermography measurements obtained in a wind tunnel experiment. The complex behavior of the

boundary layer, where laminar-turbulent transition occurs over a laminar separation bubble, complicates the data analysis of these measurements with respect to attached flow conditions, in particular when unsteady aerodynamic effects have to be considered. Insights into the flow physics from a CFD analysis of the wing geometry were therefore used to support the analysis and interpretation of the experimental data. The laminar-turbulent boundary layer transition location was determined for a range of angles of attack in steady inflow and for one test case with unsteady inflow based on the infrared thermography measurements, whereas the determination of the separation and reattachment locations of the laminar separation bubble based on the experimental data was found to be more challenging. The deformation of the wing shape that occurs between the ribs of the investigated wing due to the flexibility of the wing skin causes considerable differences in the boundary layer transition behavior across the span for positive angles of attack. Near the locations of the ribs, the behavior of the design shape is preserved and a relatively long laminar separation bubble forms around mid-chord, moving upstream with increasing angle of attack. Between the ribs, the distorted airfoil shape produces a small region of separated flow close to the leading edge, downstream of which the flow reattaches in a turbulent state. The spanwise extent of this effect increases with increasing angle of attack. Because this complex boundary layer behavior deviates strongly from the aerodynamic behavior of the design shape of the wing, it is recommended to dedicate more attention to preserving the sectional wing shape on highly flexible wing designs in the future, with a particular emphasis on maintaining a smooth shape in the region of the leading edge.

References

1. Avin, O., Raveh, D.E., Drachinsky, A., Ben-Shmuel, Y., Tur, M.: Experimental aeroelastic benchmark of a very flexible wing. *AIAA J.* **60**, 1745–68 (2022). <https://doi.org/10.2514/1.J060621>
2. Riso, C., Cesnik, C.E.: Correlations between UM/NAST nonlinear aeroelastic simulations and the pre-Pazy wing experiment. In: *AIAA Scitech 2021 Forum, Virtual Event*, Paper No. 1712 (2021). <https://doi.org/10.2514/6.2021-1712>
3. Goizueta, N., Wynn, A., Palacios, R., Drachinsky, A., Raveh, D.E.: Flutter predictions for very flexible wing wind tunnel test. *J. Aircr.* **59**, 1082–97 (2022). <https://doi.org/10.2514/1.C036710>
4. Mertens, C., Costa Fernández, J.L., Sodja, J., Sciacchitano, A., van Oudheusden, B.W.: Integrated aeroelastic measurements of the periodic gust response of a highly flexible wing. In: *International Forum on Aeroelasticity and Structural Dynamics IFASD, Madrid, Spain* (2022)
5. Carlomagno, G.M., Cardone, G.: Infrared thermography for convective heat transfer measurements. *Exp. Fluids* **49**, 1187–218 (2010). <https://doi.org/10.1007/s00348-010-0912-2>
6. Wolf, C.C., Gardner, A.D., Raffel, M.: Infrared thermography for boundary layer transition measurements. *Meas. Sci. Technol.* **31**(112002) (2020). <https://doi.org/10.1088/1361-6501/aba070>

7. Schwamborn, D., Gerhold, T., Heinrich, R.: The DLR TAU-code: recent applications in research and industry. European Conference on Computational Fluid Dynamics ECCOMAS, Delft, The Netherlands (2006)
8. Fehrs, M.: Boundary layer transition in external aerodynamics and dynamic aeroelastic stability. Dissertation, TU Braunschweig, ISSN 1434-8454, ISRN DLR-FB-2018-11, also NFL-FB 2017-27, Braunschweig (2018)
9. Fehrs, M., Ritter, M., Helm, S., Mertens, C.: CFD simulations of the Pazy wing in support of the third aeroelastic prediction workshop. In: International Forum on Aeroelasticity and Structural Dynamics IFASD, Madrid, Spain (2022)
10. Grille Guerra, A., Mertens, C., Little, J.C., van Oudheusden, B.W.: Investigation of the unsteady behaviour of a laminar separation bubble using infrared thermography. In: 20th International Symposium on Application of Laser and Imaging Techniques to Fluid Mechanics, Lisbon, Portugal (2022)